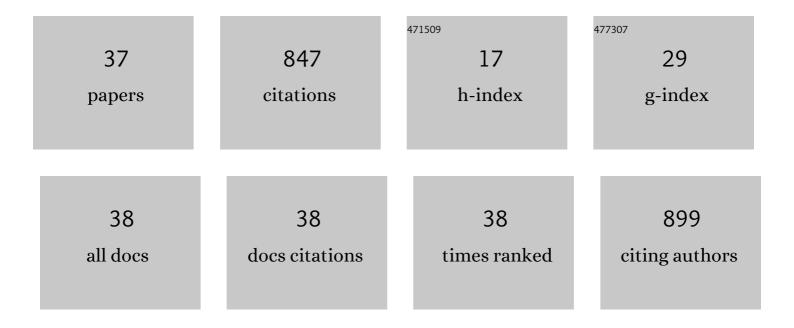
## Yuanming Pan

List of Publications by Year in descending order

Source: https://exaly.com/author-pdf/6795551/publications.pdf Version: 2024-02-01



#	Article	IF	CITATIONS
1	Electron Paramagnetic Resonance and Synchrotron X-ray Absorption Spectroscopy for Highly Sensitive Characterization of Calcium Arsenates. Environmental Science & Technology, 2022, 56, 5563-5571.	10.0	4
2	Silurian-Devonian granites and associated intermediate-mafic rocks along the eastern Kunlun Orogen, western China: Evidence for a prolonged post-collisional lithospheric extension. Gondwana Research, 2021, 89, 131-146.	6.0	15
3	Uranyl binding mechanism in microcrystalline silicas: A potential missing link for uranium mineralization by direct uranyl co-precipitation and environmental implications. Geochimica Et Cosmochimica Acta, 2021, 292, 518-531.	3.9	16
4	Crystal structure and magnetic properties of the magnetically isolated zigzag chain in KGaCu(PO <sub>4</sub> ) <sub>2</sub> . Dalton Transactions, 2021, 50, 7835-7842.	3.3	4
5	In situ X-ray diffraction study of chrysotile at high P–T conditions: transformation to the 3.65Âà phase. Physics and Chemistry of Minerals, 2021, 48, 1.	0.8	0
6	Molecular Structure of Molybdate Adsorption on Goethite at pH 5–8: A Combined DFT + U, EXAFS, and Ab Initio XANES Study. Journal of Physical Chemistry C, 2021, 125, 22052-22063.	3.1	2
7	Rational Design of (NH4 )Cu[PO4 ] with a Spin Gapped, Distorted Honeycomb Layer. European Journal of Inorganic Chemistry, 2020, 2020, 1286-1292.	2.0	3
8	Sequestration of Selenite and Selenate in Gypsum (CaSO <sub>4</sub> ·2H <sub>2</sub> O): Insights from the Single-Crystal Electron Paramagnetic Resonance Spectroscopy and Synchrotron X-ray Absorption Spectroscopy Study. Environmental Science & Technology, 2020, 54, 3169-3180.	10.0	27
9	Green synthesis and characterization of zeolite silicalite-1 from recycled mother liquor. Microporous and Mesoporous Materials, 2020, 303, 110247.	4.4	12
10	Mechanism of Gd3+ uptake in gypsum (CaSO4·2H2O): Implications for EPR dating, REE recovery and REE behavior. Geochimica Et Cosmochimica Acta, 2019, 258, 63-78.	3.9	13
11	Uptake and speciation of uranium in synthetic gypsum (CaSO 4 •2H 2 O): Applications to radioactive mine tailings. Journal of Environmental Radioactivity, 2018, 181, 8-17.	1.7	22
12	BaCu(OH) <sub>3</sub> Cl: a new one-dimensional Mott insulator with a CuO <sub>2</sub> chessboard layer. New Journal of Chemistry, 2018, 42, 18077-18083.	2.8	1
13	Controls on the formation of Cu-rich magmas: Insights from the Late Triassic post-collisional Saishitang complex in the eastern Kunlun Orogen, western China. Lithos, 2017, 278-281, 400-418.	1.4	14
14	A possible genetic relationship between orogenic gold mineralization and post-collisional magmatism in the eastern Kunlun Orogen, western China. Ore Geology Reviews, 2017, 81, 342-357.	2.7	42
15	KB(PO <sub>4</sub> )F: a novel acentric deep-ultraviolet material. Dalton Transactions, 2017, 46, 1677-1683.	3.3	40
16	Perfect Kagomé lattices in YCu <sub>3</sub> (OH) <sub>6</sub> Cl <sub>3</sub> : a new candidate for the quantum spin liquid state. Journal of Materials Chemistry C, 2016, 4, 8772-8777.	5.5	46
17	New hydrothermal route for the synthesis of high purity nanoparticles of zeolite Y from kaolin and quartz. Microporous and Mesoporous Materials, 2016, 232, 77-85.	4.4	43
18	Novel phosphate halides BaMnIII[PO4]FCl and BaMnIII[PO4]F2: Effects of mixed halides on crystal structures and magnetic properties. Journal of Solid State Chemistry, 2016, 234, 29-35.	2.9	5

YUANMING PAN

#	Article	IF	CITATIONS
19	Synthesis and magnetic properties of centennialite: a new SÂ=½ Kagomé antiferromagnet and comparison with herbertsmithite and kapellasite. Physics and Chemistry of Minerals, 2016, 43, 127-136.	0.8	21
20	Synthesis and characterization of mixed-valence manganese fluorophosphate and analogues with clathrate-like structures: Mn <sup>III</sup> <sub>6</sub> F <sub>12</sub> (PO <sub>3</sub> (OH)) <sub>8</sub> [Na <sub>8</sub> (K <s (M<sup>IV</sup> = Mn, Ti, Ge). Dalton Transactions, 2015, 44, 7960-7966.</s 	ub>X<3sub>	·(H <sup>5</sup> /sub>3
21	Synthesis and characterization of novel barium iron phosphates: Insight into new structure types tailored by hydrogen atoms. Journal of Solid State Chemistry, 2014, 212, 48-57.	2.9	19
22	Early Paleozoic high-Mg diorite-granodiorite in the eastern Kunlun Orogen, western China: Response to continental collision and slab break-off. Lithos, 2014, 210-211, 129-146.	1.4	76
23	Strong spin frustration from isolated triangular Cu( <scp>ii</scp> ) trimers in SrCu(OH) <sub>3</sub> Cl with a novel cuprate layer. Journal of Materials Chemistry C, 2014, 2, 8170-8178.	5.5	17
24	Hydrothermal synthesis of high purity zeolite A from natural kaolin without calcination. Microporous and Mesoporous Materials, 2014, 199, 50-56.	4.4	66
25	Arsenic Speciation in Newberyite (MgHPO <sub>4</sub> ·3H <sub>2</sub> O) Determined by Synchrotron X-ray Absorption and Electron Paramagnetic Resonance Spectroscopies: Implications for the Fate of Arsenic in Green Fertilizers. Environmental Science & Technology, 2014, 48, 6938-6946.	10.0	12
26	Retention and chemical speciation of uranium in an oxidized wetland sediment from the Savannah River Site. Journal of Environmental Radioactivity, 2014, 131, 40-46.	1.7	37
27	73Ge, 17O and 29Si hyperfine interactions of the center in crystalline SiO2. Journal of Magnetic Resonance, 2013, 233, 7-16.	2.1	17
28	Arsenic Incorporation in Synthetic Struvite (NH <sub>4</sub> MgPO <sub>4</sub> ·6H <sub>2</sub> O): A Synchrotron XAS and Single-Crystal EPR Study. Environmental Science & Technology, 2013, 47, 12728-12735.	10.0	30
29	Arsenic speciation in synthetic gypsum (CaSO4·2H2O): A synchrotron XAS, single-crystal EPR, and pulsed ENDOR study. Geochimica Et Cosmochimica Acta, 2013, 106, 524-540.	3.9	37
30	Hygroscopic La[B5O8(OH)]NO3·2H2O: Insight into the evolution of borate fundamental building blocks. Journal of Solid State Chemistry, 2013, 206, 91-98.	2.9	24
31	Iron pairs in beryl: New insights from electron paramagnetic resonance, synchrotron X-ray absorption spectroscopy, and ab initio calculations. American Mineralogist, 2013, 98, 1745-1753.	1.9	15
32	Investigation on pseudosymmetry, twinning and disorder in crystal structure determinations: Ba(H2O)M2III[PO3(OH)]4 (M=Fe, V) as examples. Journal of Solid State Chemistry, 2012, 187, 89-96.	2.9	12
33	Electron paramagnetic resonance spectroscopy of Fe3+ ions in amethyst: thermodynamic potentials and magnetic susceptibility. Physics and Chemistry of Minerals, 2011, 38, 159-167.	0.8	46
34	Synthesis and crystal structure of a new open-framework iron phosphate (NH4)4Fe3(OH)2F2[H3(PO4)4]: Novel linear trimer of corner-sharing Fe(III) octahedra. Journal of Solid State Chemistry, 2010, 183, 2763-2769.	2.9	16
35	Hemimorphite as a natural sink for arsenic in zinc deposits and related mine tailings: Evidence from single-crystal EPR spectroscopy and hydrothermal synthesis. Geochimica Et Cosmochimica Acta, 2010, 74, 2943-2956.	3.9	16
36	Radiation-induced defects in quartz. III. Single-crystal EPR, ENDOR and ESEEM study of a peroxy radical. Physics and Chemistry of Minerals, 2009, 36, 61-73.	0.8	31

#	Article	IF	CITATIONS
37	Radiation-damage-induced defects in quartz. I. Single-crystal W-band EPR study of hole centers in an electron-irradiated quartz. Physics and Chemistry of Minerals, 2008, 35, 103-115.	0.8	41